Chorus and hiss scales in the inner magnetosphere: statistics from high-resolution filter bank (FBK) Van Allen Proves multi-point measurements

O. Agapitov[1,2], D. Mourenas[3,4], A. Artemyev[5], A. Breneman[6], J.W. Bonnell[1], G. Hospodarsky[7], J. Wygant[6]

[1] Space Sciences Laboratory, University of California Berkeley, Berkeley, CA

[2]Astronomy and Space Physics Department, National Taras Shevchenko University of Kyiv, Kyiv, Ukraine

[3] CEA, DAM, DIF, Arpajon, France

[4] Université Paris-Saclay, CEA, Laboratoire Matière en Conditions Extrêmes, Bruyères-le-Châtel, France

[5] UCLA, Los Angeles, CA, USA

[6]University of Minnesota

[7] University of Iowa

We use Van Allen Probes FBK VLF wave data (2013-2019) to investigate the spatial extent of active regions of chorus and hiss waves

The correlation of chorus wave power is found to remain significant up to inter-spacecraft separations of 400 km to 750 km transverse to B0

Abstract

The spatial scales of whistler-mode waves, determined by their generation process, propagation, and damping, are important for assessing the scaling and efficiency of wave-particle interactions affecting the dynamics of the radiation belts. We use multi-point wave measurements in 2013-2019 by two identically equipped Van Allen Probes spacecraft covering all MLTs at L=2-6 near the geomagnetic equator to investigate the spatial extent of active regions of chorus and hiss waves, their wave amplitude distribution in the source/generation region, and the scales of chorus wave packets, employing a time-domain correlation technique to the spacecraft approaches closer than 1000 km, which happened every 70 days in 2012-2018 and every 35 days in 2018-2019. The correlation of chorus wave power dynamics using two spacecraft measurements is found to remain significant up to inter-spacecraft separations of 400 km to 750 km transverse to the background magnetic field direction, consistent with previous estimates of

the chorus wave packet extent, but indicating the likely presence of two different scales of about 400 km and 750 km. Our results further suggest that the chorus source region can be slightly asymmetrical, more elongated in either the azimuthal or radial direction, which could also explain the aforementioned two different scales. An analysis of average chorus and hiss wave amplitudes at separate locations similarly reveals different radial and azimuthal extents of the corresponding wave active regions, complementing previous results based on THEMIS spacecraft statistics mainly at larger L>6. Both the chorus source region scale and the chorus active region size appear smaller inside the outer radiation belt (at L< 6) than at higher L-shells.

1. Introduction

Chorus emissions are known to have a multi-scale spatial structure: (a) the largest spatial parameter is the chorus active region - the region in the magnetosphere where chorus activity with similar frequency and amplitude is observed simultaneously. This region was estimated by Agapitov et al. (2018) to be about 1 R_E in the morning and day sectors of the inner magnetosphere and to be 2-5 times smaller in the night sector. (b) The spatial extent of a single chorus element – the maximal distance transverse to the background magnetic field direction where the same chorus wave packet can be detected simultaneously by two spacecraft. This scale was estimated to be ~600-800 km at L~4-6 from Cluster measurements (Agapitov et al., 2011), Van Allen Probes waveforms processing (Agapitov et al., 2017; Shen et al., 2019) and from wave amplitude difference analysis (Aryan et al., 2017). THEMIS data (Agapitov et al., 2018) at larger L indicate that this scale is even larger in the outer magnetosphere. This corresponds closely to the high level of chorus time coherency (Ma et al., 2014), suggesting that the source spatial scales are much greater than the wavelength (which is of the order of 10 km in the inner magnetosphere). However, if plasma density is high (in the vicinity of the plasmapause, for example) the wavelength can be just few kilometers and the spatial extent of a single chorus element, presumably, can be smaller (Santolik et al., 2003; Santolík and Gurnett, 2003; Santolik et al., 2004). Within the spatial extent of a single chorus element (b) we define two subscales. The first is the distance r_{ampl} over which wave amplitude decays to half of its maximal value. r_{ampl} was estimated by Agapitov et al., 2018 to be about 200-300 km. The second is the coherence scale, defined as the distance at which waveforms recorded by two spacecraft have a constant time shift during a time interval greater than the wave period. This scale is important for

the efficiency of nonlinear wave-particle interactions. Estimations based on Cluster and Van Allen Probes measurements showed that this scale can vary from 60 to 300 km (Agapitov et al., 2010, 2011, 2017; Zhang et al., 2020), and presumably depends on the distance from the source and the plasma density fluctuation level (Agapitov et al., 2010, 2011).

We present the statistical results of chorus and hiss source and active region scales obtained from more than 6 years of the Van Allen Probes magnetic and electric field filter bank (FBK) data. The FBK data includes measurements of one component wave amplitude of electric and magnetic field (a shared data channel with EMFISIS). The magnetic field component, contrary to the electric field measurements was not spin modulated, which makes it suitable for a correlation analysis. These provided continuous measurements of the peak magnetic and electric field amplitudes at 8 s^{-1} sampling rate in 7 (13) frequency channels logarithmically spaced from 0.8 to 6500 Hz (e.g. Tyler et al., 2019). The measurement mode changed during the mission: the measurements modes are listed in Table 1 for more details. This work is supplementing previous studies based on more sparse Van Allen Probes waveform data (Agapitov et al., 2017; Shen et al 2019), by examining the much longer time series of FBK whistler-mode wave measurements.

Table 1. EFW Filter Bank Modes. E_{12} is the electric field from the Van Allen Probes electric field antennas 1 and 2; SCM_w is magnetic field

Time period	The FBK Mode	
2012-09-01 to 2013-03-16	13 channels from E_{12} (Channels #1-13)	
2013-03-16 to 2018-04-13	7 channels from E_{12} 7 channels from SCM_w (Channels #1,3,5,7,9,11,13)	
2018-04-14 to mission end	13 channels from E_{12} and 13 channels from SCM_{12} (Channels #1-13)	
FBK Frequency Channels Characteristics: the central (peak response) frequency and the channel width		
#1 - 1.36 Hz (0.8-1.5 Hz)	#5 – 20.8 Hz (12.0-25.0 Hz)	#9 - 334 Hz (200-400 Hz)
#2 – 2.62 Hz (1.5-3.0 Hz)	#6 – 40.6 Hz (25.0-50.0 Hz)	#10 - 658 Hz (400-800 Hz)
#3 – 5.14 Hz (3.0-6.0 Hz)	#7 – 83.8 Hz (50.0-100 Hz)	#11- 1360 Hz (800-1600 Hz)
#4 – 10.0 Hz (6.0-12.0 Hz)	#8 – 172 Hz (100-200 Hz)	#12 - 2800 Hz (1600-3200 Hz)
		#13 - 5600 Hz (3200-6500 Hz)

2. Data description

The two identically equipped NASA's Van Allen Probes spacecraft (Mauk et al., 2013), launched on 30 August, 2012, provided a suite of plasma and field measurements in the Earth's radiation belts. The two spacecraft were in near-identical orbits with an apogee near 6 R_E and a period of ~9 hours. The along-track spacecraft separation varied in time, with one spacecraft lapping the other every ~70 days during the primary mission and every ~36 days after 2018. This allows measurements from the two spacecraft to be obtained at a range of separations from ~100 km up to multiple R_E. Electric and magnetic field waveforms are provided by the Electric Fields and Waves (EFW) instrument transmitted with the 16384 s^{-1} sampling (Wygant et al., 2013) and the Electric and Magnetic Field Instrument Suite and Integrated Science (EMFISIS) instrument with 35000 s^{-1} sampling (Kletzing et al., 2013). EMFISIS FluxGate Magnetometer (FGM) measurements were used for the background magnetic field estimation. Unlike sporadic burst data, the continuous 8 s-1 filter bank magnetic field wave power measurements (FBK) allow straightforward statistical analysis of chorus and hiss structures. An example of FBK measurements from both Van Allen Probes is presented in Figure 1a,b. The inter-spacecraft distance during this spacecraft approach event is shown in Figure 1c. The correlation coefficient between wave power in the chorus frequency range (channel 6, frequency range from 600 to 1600 Hz) measured by the two separate spacecraft, is estimated by calculating correlations between simultaneous chorus wave intervals of 10 s. This correlation coefficient is provided in Figure 1d, showing a significant correlation up to 0.8-0.85 at an inter-spacecraft separation of 450-500 km. This result is verified by comparison to a similar analysis of the burst waveform data for the same time interval presented by Agapitov et al. (2017). The dynamic spectra from Van Allen Probes A and B waveform data, presented in Figure 1e,f, show the rising tone structure of chorus emissions in the 760-1100 Hz frequency range. This fine time structure is well reproduced by the FBK data shown in Figure 1g, confirming the reliability of the FBK data with 8 s^{-1} sampling rate for analyzing the chorus wave packet structure and the scale of the chorus source region.

Figure 2a,b shows the data coverage of Van Allen Probes data and close approaches, respectively. Coverage is uniform in MLT, with but significantly better in the *L*-shell range from 4 to 6.5. The distribution of measurements in the ΔMLT-ΔL domain for chorus and hiss show sufficient inter-spacecraft azimuthal coverage (ΔMLT) but a lack of measurements for radial inter-spacecraft distances greater than 0.5 R_E (with ΔMLT<1).

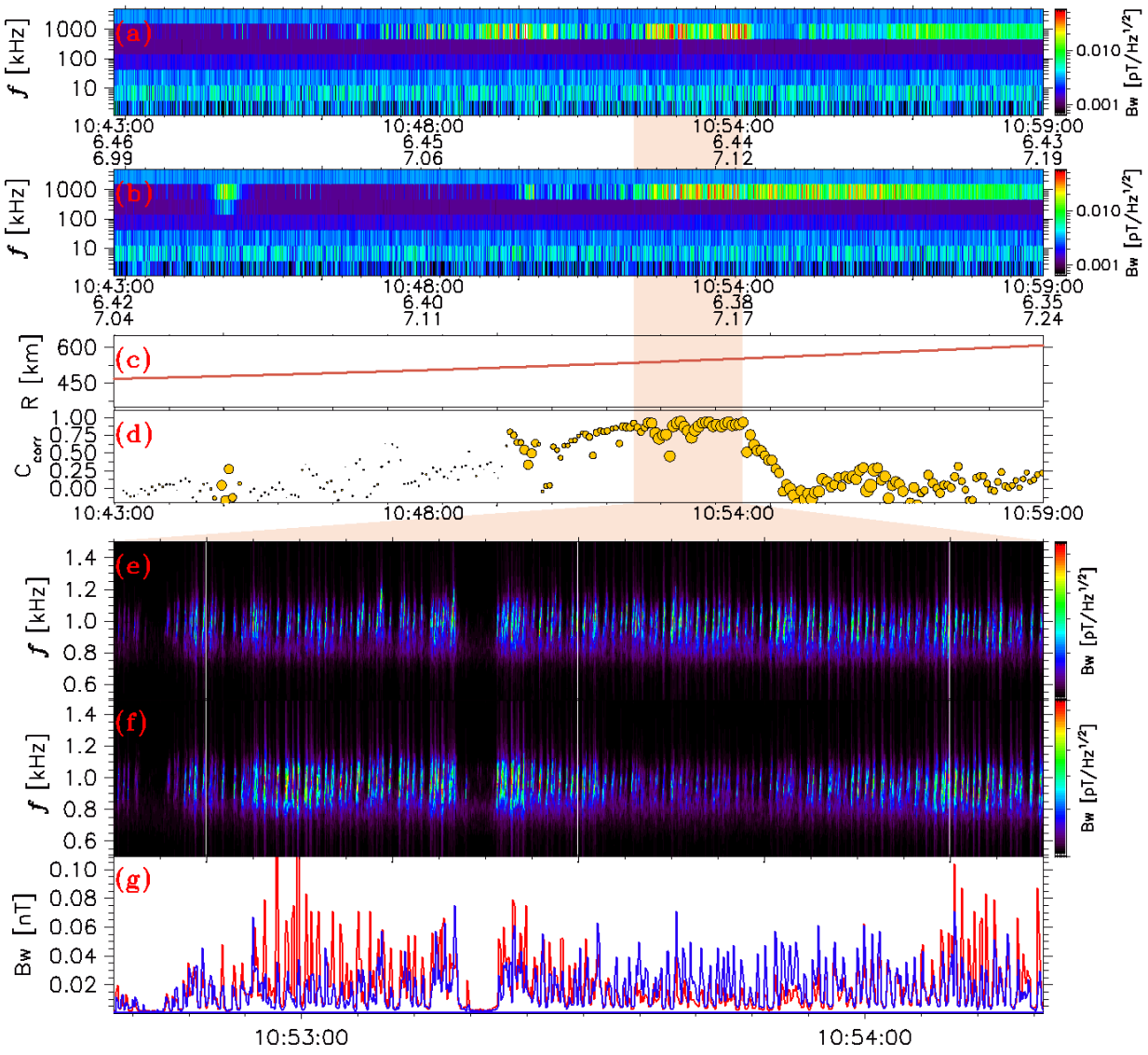

Figure 1. The electric field wave experiment (EFW) filter bank (FBK) magnetic field spectrograms recorded by Van Allen Probe A (a) and B (b) at L-shell about 6.4 in the morning sector of the magnetosphere (around 0700 MLT) on July 15, 2014. The inter-spacecraft separation (primarily azimuthal) is shown in panel (c). The dynamics of the correlation coefficient estimated for FBK wave power dynamics for 10 sec intervals is presented in panel (d). The circle size corresponds to the wave amplitude (see the legend). Panels (e) and (f) represent the dynamic spectra evaluated from the waveform data recorded by Van Allen Probes A and B respectively. The corresponding wave power from the FBK data set (the fifth channel of 800-1500 Hz) is presented in panel (g) by the red (Van Allen Probe A) and blue (Van Allen Probe B) curves.

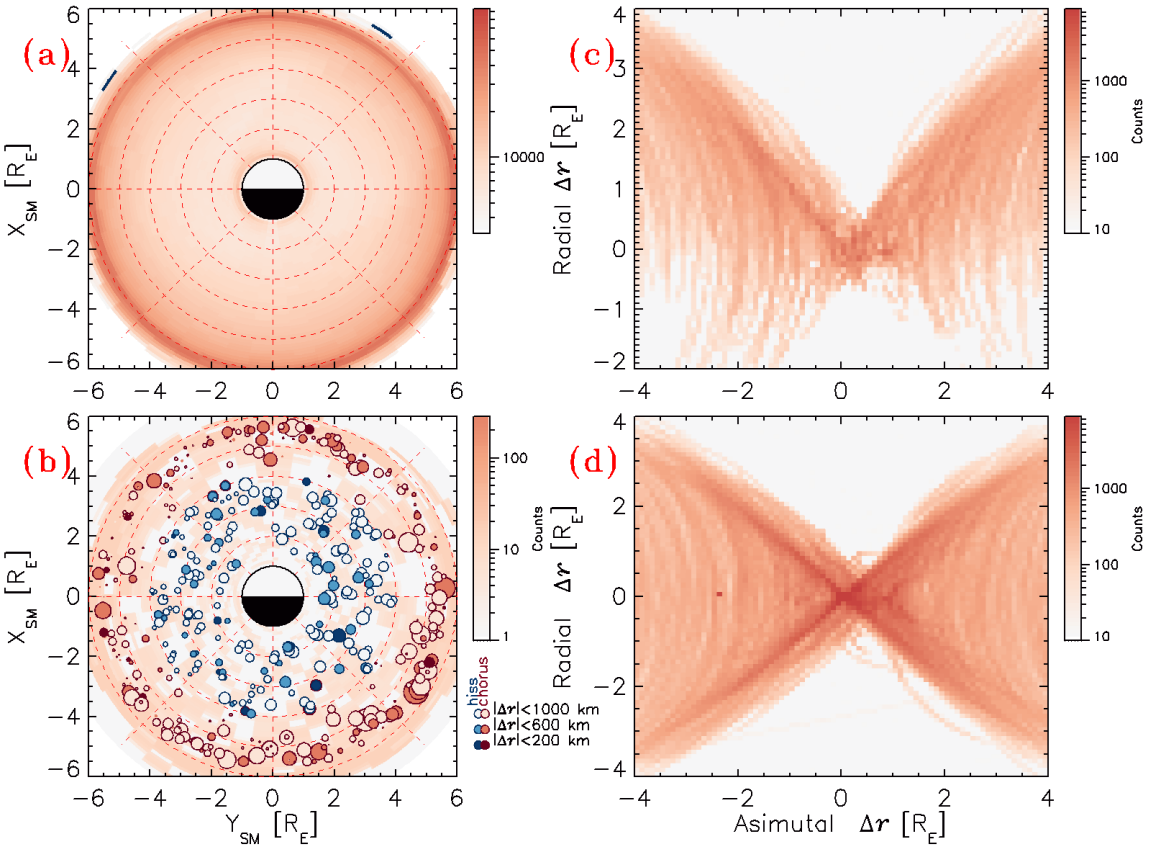

Figure 2. (a) - coverage of Van Allen Probes FBK measurements from 2013-2018. (b) - distribution (in number of minutes) of Van Allen Probes FBK measurements at relative separations between the two Van Allen Probes less than 1000 km. The closest approaches (during one hour) of the spacecraft are marked by circles, with circle size corresponding to the observed averaged wave amplitudes. The circles colors indicate the minimal separation during each hour. Red and blue color circles denote chorus and hiss waves, respectively. Panels (c) and (d) present the distributions of the inter-spacecraft separations in the ΔMLT-Δ*L* domain for chorus and hiss, respectively.

3. Chorus spatial scales

The distribution of the correlation coefficient, calculated using the same method as in Figure 1d, is presented in Figure 3a. The results are shown for two different types of measurements: for low wave amplitudes < 3 pT near noise level (blue marks) and for significant wave amplitudes above

3 pT (red marks). The correlation coefficients are provided as a function of inter-spacecraft distance ($\Delta r_\perp$) in Figure 3a, showing (i) the 95% confidence interval of the entire distribution of correlation coefficients at a given inter-spacecraft distance (error bar), and (ii) the 95% confidence interval of the correlation coefficient mean value calculated during each close encounter of the Van Allen Probes (error box). Cuts of the distribution from Figure 3a are presented in Figure 3c,e,g,i for different inter-spacecraft separations. Correlations between high amplitude chorus signal dynamics (red) are much higher than correlations between uncorrelated noisy signals (blue) for $\Delta r_\perp$ between 100 km and 800 km, suggesting that such correlations are real. To assess more quantitatively the statistical significance of these correlations, we compare in Figures 3d,f,h,j the probability $P(R>R_0)$ to reach a correlation $R > R_0$ (that is, the complementary to the cumulated distribution function) for correlations between high-amplitude chorus signals (red curves), and for *apparent* correlations between *uncorrelated noisy wave signals* (blue curves). The latter provide an estimate of *chance* correlations, that is, of correlation levels which can be reached between two series of *low-amplitude noisy signals*. When the probability of a given correlation R between high amplitude chorus signals is more than 10 times higher than the probability to obtain this correlation by chance (based on the apparent correlations found between uncorrelated noisy signals), this correlation can be considered as statistically significant. The domains of statistically significant correlations (defined as $cc>0.5$) are highlighted by reddish zones in Figures 3d,f,h,i. Figures 3d,f,h,j show that for $\Delta r_\perp$ = 200 km to 700 km, statistically significant correlations are found above an approximate level of R = 0.5, whereas for $\Delta r_\perp$ = 1400 km no significant correlations exist anymore. Based on these results, we can now examine Figure 3a in more details.

Figure 3a shows the presence of a strong correlation between high amplitude chorus signals for an inter-spacecraft distance $\Delta r_\perp$ varying from 50 km to 400 km, with a statistically significant mean correlation coefficient R above 0.6. In the $\Delta r_\perp$ range from 400 km to 750 km, the mean correlation value spreads, suggesting the likely presence of a distribution containing two different scales: a first distribution with a statistically significant mean correlation coefficient remaining above 0.5 for $\Delta r_\perp$ up to 750 km, and a second distribution with a vanishing (non-significant) correlation when $\Delta r_\perp$ increases above 400 km. The distributions of correlation coefficients presented in Figure 3c,e,g,i for different inter-spacecraft distances show that at distances above 400 km, a significant part of the 10-second intervals of high-amplitude chorus

waves are indeed uncorrelated (see the overlapping red and blue parts). Figure 3j further shows that at an inter-spacecraft distance of 1400 km or more, the correlation coefficients calculated between high-amplitude chorus signals and between uncorrelated noisy signals are similarly Gaussian-like distributed around a zero mean value, indicating the absence of any significant correlation between high-amplitude chorus waves at such large inter-spacecraft distances. The present FBK statistics of chorus wave amplitude dynamics therefore show the presence of two characteristic scales for the source region of chorus wave packets of ~400 km and ~750 km, respectively.

The present results on the spatial extent of the source region of chorus waves correspond well to the previous results obtained based on THEMIS data for lower and higher amplitude waves (Agapitov et al., 2018): lower amplitude chorus waves were found to have larger source scales ~600-800 km, whereas the source region of higher amplitude chorus waves was found to be much more localized ~300-400 km. However, no clear amplitude dependence was found when using Van Allen Probes data, possibly due to the more limited L-shell range of close approaches of the Van Allen Probes A and B spacecraft, since all the results are obtained in the *L*-shell range from 5 to 6 and only 42 close approaches with significant wave activity are available. An alternative explanation for the two scales ~ could be the existence of separate in the azimuthal and radial directions. This possibility will be examined in more detail below.

Other estimates of the chorus source region scale obtained from the processing of microbursts scales based on low Earth orbit electron flux measurements suffer from the same limitation of using only two points measurements and, in addition, the AC-6 (Shumko et al., 2020) and FIREBIRD (Breneman et al., 2017; Shumko et al., 2018) CubeSat correlations are mostly provided when the spacecraft pair is separated in the radial direction. Estimates of the radial and azimuthal equatorial chorus scales during one event were provided by Shumko et al. (2018) based on the bouncing relativistic electron flux (presumably accelerated/generated by chorus waves), and were found to be close (530±10 and 500±10 km respectively). Microbursts scales are presumably related to the distribution of wave amplitude inside the chorus source (Shumko et al., 2020), since microbursts are likely produced when the amplitude of whistler-mode waves exceeds a threshold for nonlinear wave-particle interaction, allowing fast precipitation loss (Artemyev et al., 2014, 2016; Chen et al., 2020; Zhang et al., 2019).

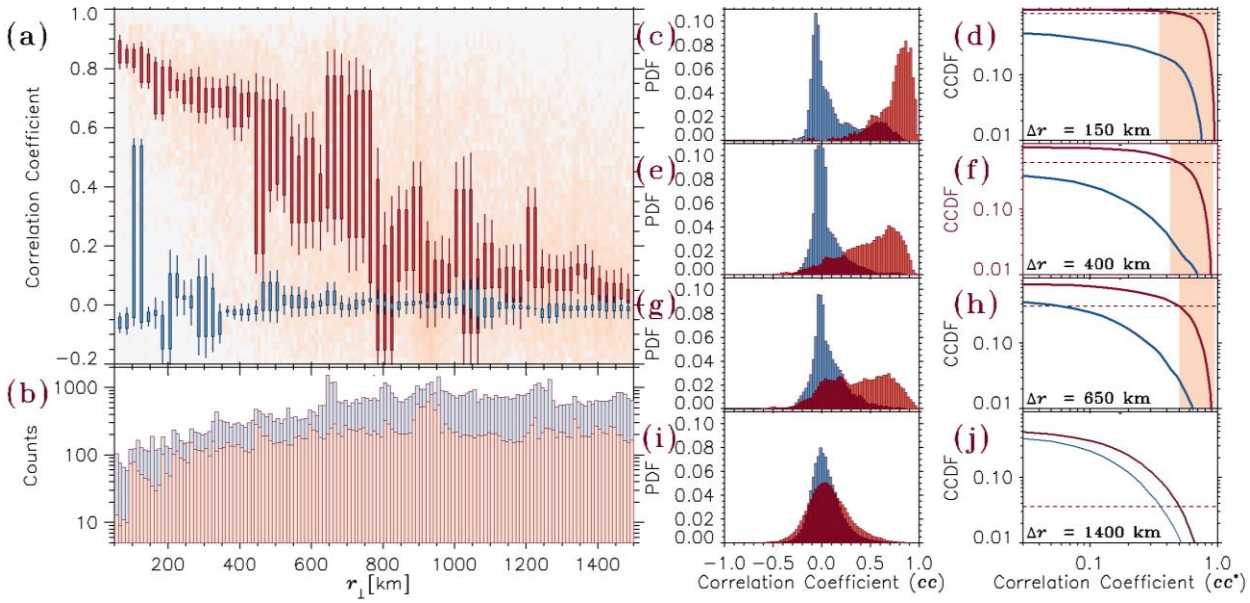

Figure 3. Distribution of the correlation coefficients calculated on 10 s intervals of the FBK measurements by Van Allen Probes A and B in the chorus wave frequency range. The 95% confidence interval for the mean correlation coefficient calculated during each close encounter of the Van Allen Probes is shown, and the error bars give the 95% confidence interval for the full distribution, both calculated based on chorus wave intervals with significant amplitudes, higher than 3 pT (red marks). Correlation coefficients calculated using intervals with low amplitude (< 3 pT) waves near the noise level are shown in blue. The total numbers of contributing time intervals is shown in panel (b) with the same corresponding colors. Panels (c,e,g,i) present cuts of the distributions in panel (a) at 150 km (c), 400 km (e), 650 km (g), and 1400 km (i). The corresponding probability $P(cc > cc^*)$ to reach obtain the correlation coefficient cc value greater than cc^* – that is, the complementary to the cumulated distribution function (CCDF(cc^*)) – is shown in panels (d,f,h,j) as a function of cc^*, separately for correlations between high-amplitude chorus signals (red curves) and for apparent correlations between uncorrelated noisy signals (blue curves). Domains of statistically significant correlations cc between high amplitude chorus dynamics are highlighted by reddish zones; they correspond to probabilities $P(cc > cc^*)$ more than 10 times higher than the probability to obtain such correlations by chance (based on the apparent correlations found between uncorrelated noisy signals). The probability of obtaining a correlation coefficient greater than 0.5 is indicated by a dashed line.

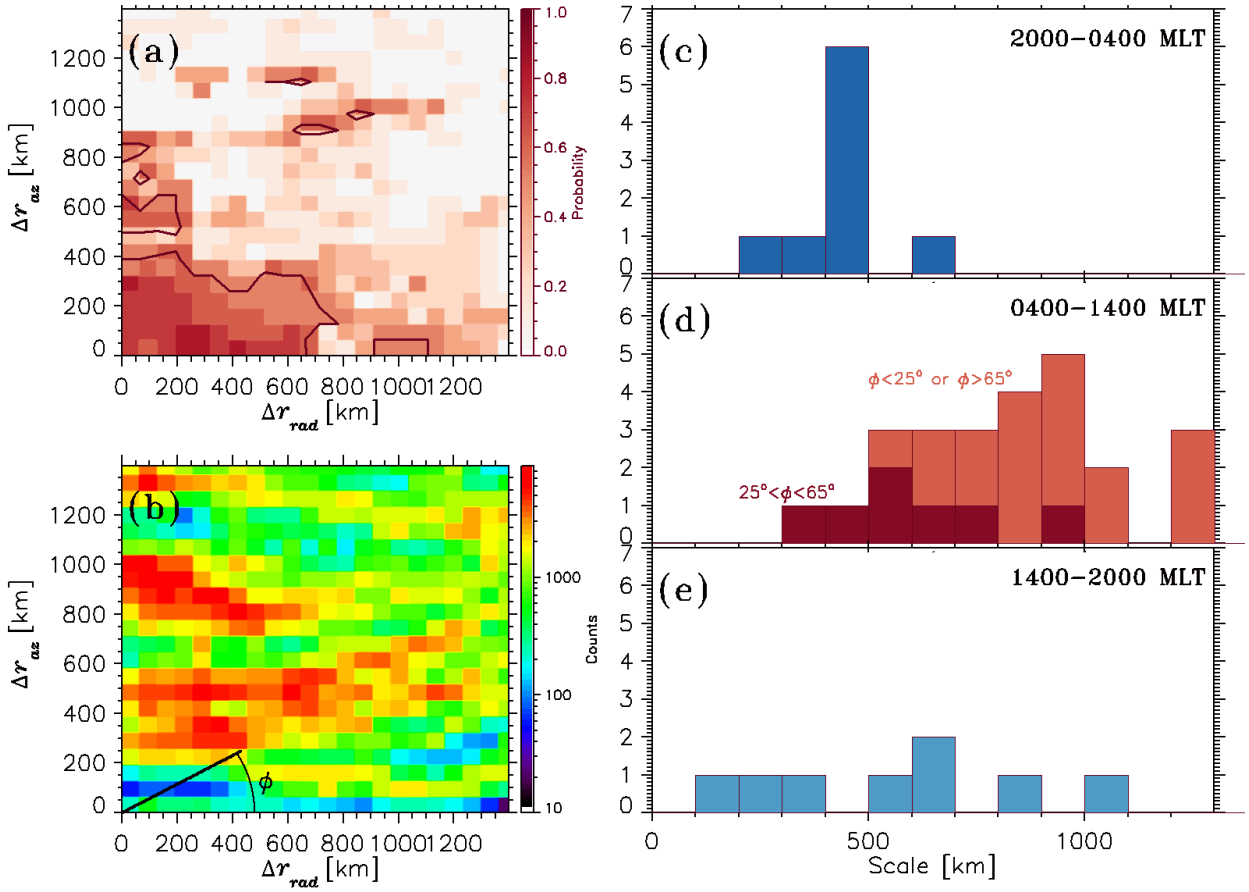

Figure 4. The distribution of the probability to get a correlation above 0.5 between high-amplitude chorus signals simultaneously recorded by the two Van Allen Probes is presented in panel (a) in the $\Delta r_{rad} - \Delta r_{az}$ domain. The solid contour shows the level of 0.5 probability – inside this contour, the correlation coefficient is greater than 0.5 in more than 50% of the cases. The total number of time intervals in this domain is shown in panel (b). The histograms of correlation scales (estimated at the correlation level of 0.5 for statistical significance) from the night-morning (2000-0400MLT), day (0400-1400MLT), and evening (1400-2000MLT) sectors are presented in panels (c,d,e), respectively. Intermediate values of the polar angle $\phi = atan\left(\frac{\Delta r_{rad}}{\Delta r_{az}}\right)$ (marked in panel (b)) are shown by dark red in panel (d).

Figure 4a presents the probability levels for cc>0.5 for the chorus source region in the domain of azimuthal and radial inter-spacecraft separation. The spatial configuration of the chorus source is almost isotropic in the azimuthal and radial directions with a slightly larger azimuthal scale $\Delta r_{\perp az}$of 900±50 km compared to 700±50 km for the radial scale $\Delta r_{\perp rad}$,

confirming the asymmetry of the chorus source found by Shen et al. (2019) based on the sparser waveform data from the Van Allen Probes. The observed shapes (with shorter correlation scale at intermediate values of polar angle $\phi = atan\left(\frac{\Delta r_{rad}}{\Delta r_{az}}\right)$, i.e. $25° < \phi < 65°$) suggest a bigger asymmetry of the source region elongated along either the radial or azimuthal directions in different cases. This cannot be fully resolved using only two-points measurements, but it is worth noting that it may also partly explain the two scales (400 km and 750 km) of the distribution of the correlation coefficients in Figure 3a.

The bulk of the estimates (25 approaches) is based on measurements in the day sector of the magnetosphere from 4 to 14 MLT. The scales obtained in this MLT sector are presented in Figure 4c. For 23 of 25 approaches the scales of chorus spatial extent were found to be larger than 500 km. The possible asymmetry of the chorus source seen in Figure 4a can again be seen in Figure 4c, where the results are presented for different ranges of ϕ. The distribution for $\phi < 25° \vee \phi > 65°$ is marked by light-red, and the distribution for $25° < \phi < 65°$ is highlighted by dark red. The scales for the first ϕ range are significantly larger than the scales obtained for intermediate values of ϕ, confirming the anisotropy of the chorus source region as a possible explanation for the results in Figure 4a (and in Figure 3a). The evening sector (14-20 MLT, 8 approaches) is presented in Figure 4d, with scales ranging from 200 km to 1000 km. The results for the night-morning sector (9 approaches) are displayed in Figure 4e, and represent the smallest obtained scales on average, mostly less than 500 km.

The parameters of the wave amplitude distribution inside the source region can be evaluated under the assumption of a Gaussian distribution $B_w = B_0 exp(-0.5r^2/\sigma^2)$(Agapitov et al., 2017). Then, the distribution of the ratio of wave amplitudes captured by the two spacecraft B_{w1}/B_{w2} can be fitted by Gaussian-based distributions, allowing us to infer the value of the parameter σ, which represents the inter-spacecraft distance r where wave amplitude decays to half its peak value. The wave amplitude ratio distribution is presented as a function of r in Figure 5a for day sector chorus waves. The value of σ that allows to best fit the distribution was found to be 330±30 km. Cuts of the distribution function, together with the corresponding Gaussian-based values are shown in Figure 5b. The obtained range of σ values encompasses the values previously obtained in (Agapitov et al., 2017) for a single Van Allen Probes A and B

close approach on July 15, 2014 (300 km). This scale σ can be directly related to the observed scales of microburts, which are presumably produced by nonlinear wave-particle interaction processes and, therefore, probably correspond to a wave amplitude threshold.

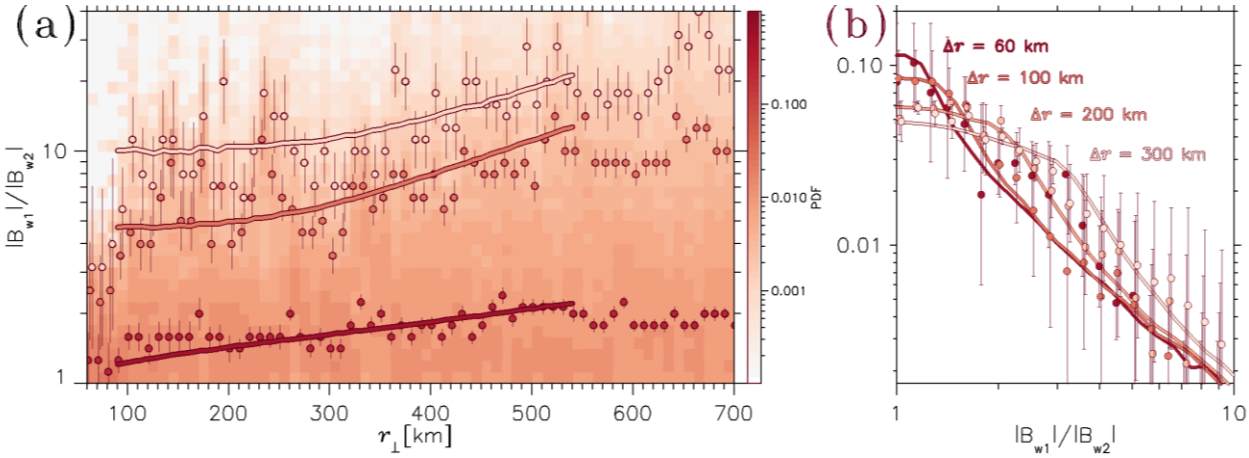

Figure 5. The distribution of the ratio of chorus wave amplitudes captured by Van Allen Probes A and B as a function of inter-spacecraft distance. The 0.75, 0.9, and 0.95 quartiles of the distribution are shown with the circles of the corresponding color**.** The dashed curves indicate the same 0.75, 0.9, and 0.95 quartiles calculated under the assumption of a Gaussian wave amplitude distribution in the source region ($B_w = B_0 exp(-0.5r^2/\sigma^2)$) with $\sigma = 330$ km. Panel (b) presents cuts of the distribution from panel (a) at distances indicated in the legend. The distributions obtained under the Gaussian assumption are shown by thin solid curves of the corresponding colors.

The spatial extent of the wave active region – the region where waves are observed simultaneously with similar characteristics – is an important parameter for estimating the global impact of wave-particle interactions in the radiation belts. Figure 6 presents the instantaneous spatial extent of the active hiss and chorus regions in the radial ΔL (a) and azimuthal ΔMLT(b) directions, respectively, in the L-MLT domain. Van Allen Probes EMFISIS measurements at L<6.5 complement the THEMIS FBK data analyzed in (Agapitov et al., 2018). The radial extent of the chorus active region is smaller at L-shells<6 than at the L-shells>6 investigated in (Agapitov et al., 2018). However, its radial and azimuthal extents are consistent with the ones determined at L>6, with maximum extents of about 1 hour in MLT and 0.5 R_E in the radial direction in the 10-15 MLT sector.

The hiss active region is significantly (~ 2-3 times) more elongated in the azimuthal direction in the post-noon sector (there reaching ΔMLT ~1.5-2.2). This difference between the pre-noon and post-noon sectors is probably due to hiss local growth vs hiss from an embryonic chorus source that enters the plasmasphere at high latitudes around noon before filling the 12-16 MLT sector (Bortnik et al., 2008; Chen et al., 2012; Meredith et al., 2013; Agapitov et al., 2018; Hartley et al., 2019).

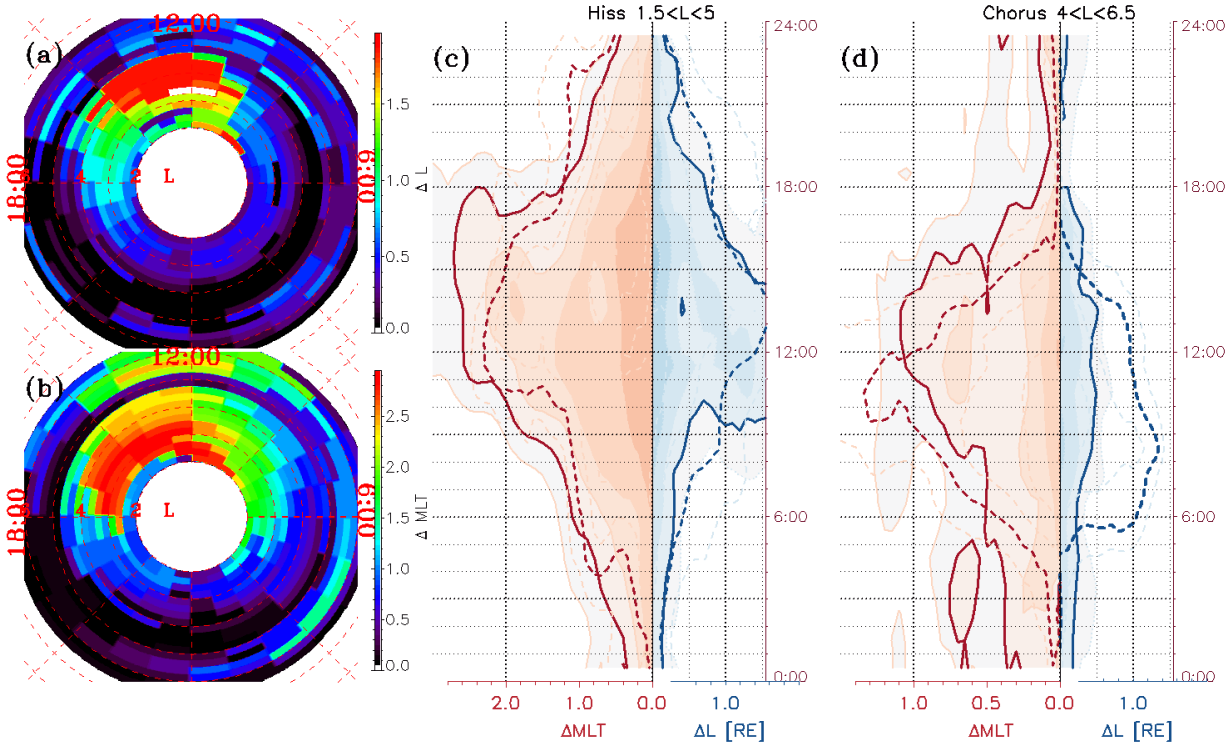

Figure 6. Spatial extent of whistler-mode waves active regions in the radial (a) and azimuthal (b) directions, determined as the maximal distance at which the waves were observed simultaneously in at least 50% of the observations with amplitudes higher than 3 pT. The spatial extents (the ΔMLT and ΔL at which the probability to observe the wave activity simultaneously aboard two spacecraft decays to 0.5) for hiss ($f_{LH} < f < 0.1f_{ce}$) and lower-band chorus ($0.1f_{ce} < f < 0.5f_{ce}$) wave active regions are shown in panels (c) and (d), respectively. Dashed lines show the spatial extents obtained from THEMIS data mainly at larger L > 6 (Agapitov et al., 2018).

5. Conclusions

We report the chorus and hiss waves spatial characteristics based on more than 6 years of continuous Van Allen Probes A and B spacecraft measurements of magnetic field wave power in

the filter bank mode (FBK). We verified that the 8 s^{-1} sampling rate is sufficient to resolve the chorus packet structure and that it allows a reconstruction of the spatial amplitude structure of the chorus source region based on two points measurements. An important advantage of using FBK data for the present statistical study is that such measurements are continuously available during the entire mission (for example, the EMFISIS burst mode data is available during less than 1% of the mission time, roughly during several 6 second intervals per hour).

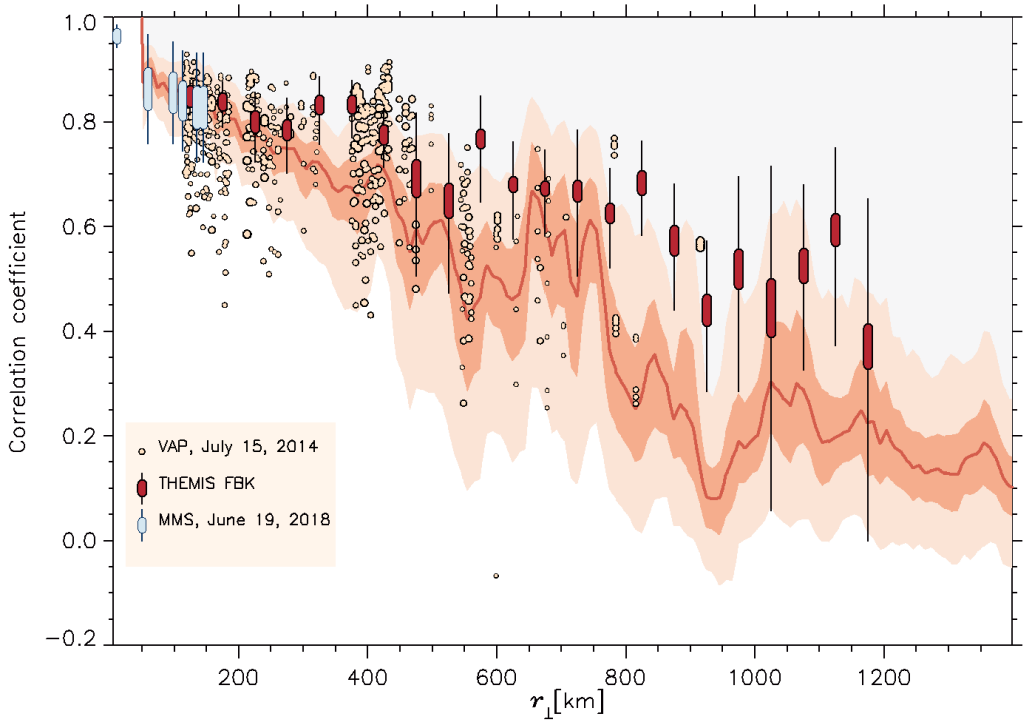

Figure 7. Median value of the correlation coefficient from the Van Allen Probes A and B statistics from Figure 3 (solid red curve). The 90% confidence interval of the median value of the correlation coefficient calculated during each close encounter of the Van Allen Probes is shown as the red curve, while the light red zone shows the 90% confidence interval of the full correlation coefficient distribution. The yellow circles show results from the Van Allen Probes A and B case study presented in (Agapitov et al., 2017). The dark red marks indicate the results obtained from THEMIS filter bank (FBK) data analysis by (Agapitov et al., 2018). The light blue marks show MMS results recorded on June 19, 2018.

The spatial extent of the chorus wave packet, that is, the transverse inter-spacecraft distance over which the same chorus element can be detected by two spacecraft simultaneously, is found to vary between 400 km and 750 km, consistent with previous results (Agapitov et al.,

2011, 2017, 2018; Shen et al., 2019). The correlation coefficient distributions from THEMIS, Van Allen Probes, and MMS spacecraft in Figure 7 show a good overall agreement, although THEMIS scales -- mainly obtained at higher *L*-shells - appear slightly larger.

The two dimensional spatial distribution of the correlation coefficient as a function of radial and azimuthal separations suggests that the chorus source can be slightly asymmetrical (with a scale ratio of about 1.4±0.3) and elongated in either azimuthal or radial direction. Investigating this asymmetry in more detail would require a further study using simultaneous measurements made at more than two points to resolve the azimuthal and radial separations simultaneously (using Cluster or MMS multi-satellite data).

The spatial distribution of the chorus wave amplitude in the source is found to be close to a Gaussian, with $B_w = B_0 exp(-0.5r^2/\sigma^2)$ and a variance $\sigma = 330 \pm 50$ km, consistent with previous results (Agapitov et al., 2017).

The active region of chorus waves (the region where chorus waves are observed simultaneously with a significant amplitude of >3 pT) is found to extend ~0.1 to 0.5 R_E in the radial direction (ΔL) and is much more elongated in the azimuthal direction (ΔMLT) where its extension varies between 0.4 and 1.2 R_E, with maximal values in the day sector – consistent with past results based on THEMIS measurements (Agapitov et al., 2018) and Van Allen Probes measurements (Aryan et al., 2016)). Van Allen Probes measurements cover well the inner magnetosphere from *L* ~ 4 to 6, usefully supplementing the good THEMIS coverage of *L*-shells above 6.

The spatial characteristics of plasmaspheric hiss waves obtained from Van Allen Probes FBK measurements show that hiss amplitude modulation can be detected at a distance of up to 3000±500 km. This confirms previous results reported by (Breneman et al., 2017; Agapitov et al., 2018). The active region of hiss waves is significantly elongated azimuthally, reaching up to 3 hours in MLT in the post-noon sector, as compared with its radial scale of ~0.5-1.5 R_E. The azimuthal correlation scale length of hiss in the 12-16 MLT post-noon sector is more than twice wider than in the 6-10 MLT pre-noon sector, consistent with local hiss wave growth in the post-noon sector from seed chorus waves entering the plasmasphere around noon (Bortnik et al., 2008; Chen et al., 2012; Meredith et al., 2013; Agapitov et al., 2018; Hartley et al., 2019). In

contrast, pre-noon hiss waves are likely generated locally by anisotropic electron injections without any seeding from chorus waves (Liu et al., 2020).

Data Availability Statement

Van Allen Probe EMFISIS data are available at the website http://emfisis.physics.uiowa.edu/data/index).

EFW waveforms and FBK data are available at the website (http://www.space.umn.edu/rbspefw-data/).

Acknowledgments

The work of O.A. was supported by National Aeronautics and Space Administration (NASA) grants 80NNSC19K0848, 80NSSC20K0218, NNX16AF85GS004, 80NSSC19K0264, and National Science Foundation (NSF) grant number 1914670.

References

Agapitov, O., V. Krasnoselskikh, Y. Zaliznyak, V. Angelopoulos, O. L. Contel, and G. Rolland (2010), Chorus source region localization in the Earth's outer magnetosphere using THEMIS measurements, *Ann. Geophys.*, *28*(6), 1377–1386.

Agapitov, O., V. Krasnoselskikh, Y. V. Khotyaintsev, and G. Rolland (2011a), A statistical study of the propagation characteristics of whistler waves observed by Cluster, *Geophys. Res. Lett.*, *38*(20).

Agapitov, O., V. Krasnoselskikh, T. Dudok de Wit, Y. Khotyaintsev, J. S. Pickett, O. Santolík, and G. Rolland (2011b), Multispacecraft observations of chorus emissions as a tool for the plasma density fluctuations' remote sensing, *J. Geophys. Res. Space Phys. 1978–2012*, *116*(A9).

Agapitov, O., V. Krasnoselskikh, Y. V. Khotyaintsev, and G. Rolland (2012), Correction to "A statistical study of the propagation characteristics of whistler waves observed by Cluster", *Geophys. Res. Lett.*, *39*(24).

Agapitov, O., A. Artemyev, V. Krasnoselskikh, Y. V. Khotyaintsev, D. Mourenas, H. Breuillard, M. Balikhin, and G. Rolland (2013), Statistics of whistler mode waves in the outer radiation belt:

Cluster STAFF-SA measurements, *J. Geophys. Res. Space Phys.*, *118*(6), 3407–3420, doi:10.1002/jgra.50312.

Agapitov, O. V., L.W. Blum, F. S. Mozer, J.W. Bonnell, and J. Wygant (2017), Chorus whistler wave source scales as determined from multipoint Van Allen Probe measurements, *Geophys. Res. Lett.*, *44*(6), 2634-2642, doi:10.1002/2017GL072701

Agapitov, O. V., D. Mourenas, A. V. Artemyev, F. S. Mozer, J.W. Bonnell, V. Angelopoulos, V. Shastun, and V. Krasnoselskikh (2018), Spatial Extent and Temporal Correlation of Chorus and Hiss: Statistical Results From Multipoint THEMIS Observations, *J. Geophys. Res. Space Phys.*, 12*3*(10), 8317-8330, doi:10.1029/2018JA025725

Artemyev, A., A. Vasiliev, D. Mourenas, O. Agapitov, and V. Krasnoselskikh (2014), Electron scattering and nonlinear trapping by oblique whistler waves: The critical wave intensity for nonlinear effects, *Phys. Plasmas, 21, 102903, doi:10.1063/1.4897945*

Artemyev, A., O. Agapitov, D. Mourenas, V. Krasnoselskikh, V. Shastun, and F. Mozer (2016), Oblique Whistler-Mode Waves in the Earth's Inner Magnetosphere: Energy Distribution, Origins, and Role in Radiation Belt Dynamics, *Space Sci. Rev.*, *200*(1–4), 261–355, doi:10.1007/s11214-016-0252-5.

Aryan, H., D. Sibeck, M. Balikhin, O. Agapitov, and C. Kletzing (2016), Observation of chorus waves by the Van Allen Probes: Dependence on solar wind parameters and scale size, *J. Geophys. Res. Space Phys.*, *121*(8), 2016JA022775, doi:10.1002/2016JA022775.

Blum, L. W., O. Agapitov, J. W. Bonnell, C. Kletzing, and J. Wygant (2016), EMIC wave spatial and coherence scales as determined from multipoint Van Allen Probe measurements, *Geophys. Res. Lett.*, *43*(10), 2016GL068799, doi:10.1002/2016GL068799.

Breneman, A., C. A. Kletzing, J. Chum, O. Santolik, D. Gurnett, and J. Pickett (2007), Multispacecraft observations of chorus dispersion and source location, *J. Geophys. Res. Space Phys.*, *112*(A5), A05221, doi:10.1029/2006JA012058.

Breneman, A. W. et al. (2015), Global-scale coherence modulation of radiation-belt electron loss from plasmaspheric hiss, *Nature*, *523*(7559), 193–195, doi:10.1038/nature14515.

405 Chen, L., A. W. Breneman, Z. Xia, and X.-J. Zhang (2020), Modeling of Bouncing Electron
406 Microbursts Induced by Ducted Chorus Waves, *Geophys. Res. Lett.*, *47*(17), e2020GL089400,
407 doi:10.1029/2020GL089400.

408 Crew, A. B. et al. (2016), First multipoint in situ observations of electron microbursts: Initial
409 results from the NSF FIREBIRD II mission, *J. Geophys. Res. Space Phys.*, *121*(6),
410 2016JA022485, doi:10.1002/2016JA022485.

411 Gurnett, D. A., R. R. Anderson, F. L. Scarf, R. W. Fredricks, and E. J. Smith (1979), Initial
412 results from the ISEE-1 and -2 plasma wave investigation, *Space Sci. Rev.*, *23*(1), 103–122,
413 doi:10.1007/BF00174114.

414 Hartley, D. P.., C. A. Kletzing, L. Chen, R. B. Horne, and O. Santolik (2019), Van Allen Probes
415 Observations of Chorus Wave Vector Orientations: Implications for the Chorus-to-Hiss
416 Mechanism, *Geophys. Res. Lett.*, *46*(5), 2337-2346, doi:10.1029/2019GL082111.

417 Helliwell, R. A. (1966), Whistlers and Related Ionospheric Phenomena, *Geophys. J. Int.*, *11*,
418 563–564, doi:10.1111/j.1365-246X.1966.tb03172.x.

419 Helliwell, R. A. (1967), A theory of discrete VLF emissions from the magnetosphere, *J.*
420 *Geophys. Res.*, *72*(19), 4773–4790, doi:10.1029/JZ072i019p04773.

421 Kletzing, C. A. et al. (2013), The Electric and Magnetic Field Instrument Suite and Integrated
422 Science (EMFISIS) on RBSP, *179*, 127–181, doi:10.1007/s11214-013-9993-6.

423 LeDocq, M. J., D. A. Gurnett, and G. B. Hospodarsky (1998), Chorus source locations from VLF
424 Poynting flux measurements with the Polar spacecraft, *Geophys. Res. Lett.*, *25*(21), 4063–4066,
425 doi:10.1029/1998GL900071.

426 Liu, N., Z. Su, Z. Gao, et al., (2020), Comprehensive Observations of Substorm-Enhanced
427 Plasmaspheric Hiss Generation, Propagation, and Dissipation, *Geophys. Res. Lett.*, *47*(2),
428 e2019GL086040, doi:10.1029/2019GL086040.

429 Mauk, B. H., N. J. Fox, S. G. Kanekal, R. L. Kessel, D. G. Sibeck, and A. Ukhorskiy (2013),
430 Science Objectives and Rationale for the Radiation Belt Storm Probes Mission, *Space Sci. Rev.*,
431 *179*(1–4), 3–27, doi:10.1007/s11214-012-9908-y.

432 Nishimura, Y. et al. (2010), Identifying the Driver of Pulsating Aurora, *Science*, *330*(6000), 81–
433 84, doi:10.1126/science.1193186.

Nishimura, Y. et al. (2011), Multievent study of the correlation between pulsating aurora and whistler mode chorus emissions, *J. Geophys. Res. Space Phys.*, *116*(A11), A11221, doi:10.1029/2011JA016876.

Omura, Y., Y. Katoh, and D. Summers (2008), Theory and simulation of the generation of whistler-mode chorus, *J. Geophys. Res. Space Phys.*, *113*, 4223, doi: 10.1029/2007JA012622.

Parrot, M., O. Santolik, N. Cornilleau-Wehrlin, M. Maksimovic, C. C. Harvey, and others (2003), Source location of chorus emissions observed by Cluster, in *Annales Geophysicae*, vol. 21, pp. 473–480.

Santolík, O., and D. A. Gurnett (2003), Transverse dimensions of chorus in the source region, *Geophys. Res. Lett.*, *30*(2), 1031, doi:10.1029/2002GL016178.

Santolik, O., D. A. Gurnett, J. S. Pickett, M. Parrot, and N. Cornilleau-Wehrlin (2003), Spatio-temporal structure of storm-time chorus, *J. Geophys. Res. Space Phys.*, *108*(A7).

Shen, X.-C., Li, W., Ma, Q., Agapitov, O., & Nishimura, Y. (2019). Statistical Analysis of Transverse Size of Lower Band Chorus Waves Using Simultaneous Multisatellite Observations. *Geophysical Research Letters*, *46*(11), 5725–5734. https://doi.org/10.1029/2019GL083118

Shumko, M., Sample, J., Johnson, A., Blake, B., Crew, A., Spence, H., et al. (2018). Microburst Scale Size Derived From Multiple Bounces of a Microburst Simultaneously Observed With the FIREBIRD-II CubeSats. *Geophysical Research Letters*, *45*(17), 8811–8818. https://doi.org/10.1029/2018GL078925

Shumko, M., Johnson, A. T., Sample, J. G., Griffith, B. A., Turner, D. L., O'Brien, T. P., et al. (2020). Electron Microburst Size Distribution Derived With AeroCube-6. *Journal of Geophysical Research: Space Physics*, *125*(3), e2019JA027651. https://doi.org/10.1029/2019JA027651

Tyler, E., Breneman, A., Cattell, C., Wygant, J., Thaller, S., & Malaspina, D. (2019). Statistical Occurrence and Distribution of High-Amplitude Whistler Mode Waves in the Outer Radiation Belt. *Geophysical Research Letters*, *46*(5), 2328–2336. https://doi.org/10.1029/2019GL082292

Trakhtengerts, V. Y. (1999), A generation mechanism for chorus emission, *Ann. Geophys.*, *17*, 95–100, doi:10.1007/s00585-999-0095-4.

Wygant, J. R. et al. (2013), The Electric Field and Waves Instruments on the Radiation Belt Storm Probes Mission, *179*, 183–220, doi:10.1007/s11214-013-0013-7.

Zhang, X.-J., Mourenas, D., Artemyev, A.V, Angelopoulos,V., Bortnik, J., Thorne, R. M., et al. (2019). Nonlinear electron interaction with intense chorus waves: Statistics of occurrence rates. Geophysical Research Letters, 46, 7182–7190.doi:10.1029/2019GL083833.